Measurement of the electron capture probabilities of ^{55}Fe with a metallic magnetic calorimeter

Martin Loidl, Matias Rodrigues, Riham Mariam

Contents lists available at ScienceDirect

Applied Radiation and Isotopes

journal homepage: www.elsevier.com

Measurement of the electron capture probabilities of ^{55}Fe with a metallic magnetic calorimeter

M. Loidl*, M. Rodrigues, R. Mariam

CEA, LIST, Laboratoire National Henri Becquerel (LNE-LNHB), CEA-Saclay, 91191 Gif/Yvette Cedex, France

ARTICLE INFO

Keywords:
Electron capture probabilities
Cryogenic detectors
Metallic magnetic calorimeters
Ionizing radiation metrology
Decay data

ABSTRACT

The ratios of the electron capture probabilities P_K, P_L and P_M of ^{55}Fe have been measured with a metallic magnetic calorimeter, a specific type of cryogenic detector. The ^{55}Fe source was enclosed in the detector absorber, whose dimensions were chosen such that the detection efficiency for Mn K X-rays was larger than 99.99%. Since all electrons and photons emitted by the source are absorbed in the detector, the detection efficiency is virtually 100% for K, L and M captures. The energy threshold was low enough to allow for clear separation of the M captures (~ 80 eV) from noise. The capture probability ratios were translated to capture probabilities using the recommended value for the probability of the undetected N captures. The resulting values are in agreement both with the recommended values of P_K, P_L and P_M and with the experimental data of Pengra and coworkers.

1. Introduction

Electron capture (EC) probabilities are among the decay data that are difficult to establish with reliability. Calculation is possible with reasonable reliability for allowed EC transitions, but calculation for forbidden transitions represents the same level of difficulty as the calculation of beta spectra for forbidden transitions. Experimental data on EC probabilities are scarce. Most of them are based on X-ray measurements, often in (anti-) coincidence with gamma-rays, and depend on the knowledge of the fluorescence yields ω_K, ω_L … Usually only P_K is determined in this way. Very few direct measurements of EC probabilities have been conducted, either using scintillator detectors with the EC nuclide embedded in the scintillator material, or by means of a proportional counter with a gaseous compound of the EC nuclide present in the counter gas. Pengra and coworkers have determined the EC probability ratios P_L / P_K and P_M / P_L for ^{55}Fe in the latter way (Pengra et al., 1972); their P_M / P_L ratio is the only existing experimental value relating to P_M.

Electron capture probabilities are required for the calculation of the detection efficiency in activity measurements of EC nuclides by liquid scintillation counting. Furthermore they are important in nuclear physics, medicine, astrophysics and other fields of fundamental research. And finally, accurate experimental data are needed to test theoretical calculations of EC probabilities. New and more accurate calculations with well-established uncertainties must be performed since not all EC probabilities can be measured, firstly in terms of experimental effort and secondly because many EC nuclides have complex decay schemes that would make the measurements very difficult to exploit. Hence a new code for the calculation of electron capture transitions is being developed (Mougeot, these proceedings). In parallel, metallic magnetic calorimeters (MMCs) have been used for the first time for the accurate determination of EC probability ratios. ^{55}Fe was chosen as the first EC nuclide to be measured, firstly because the result can be compared with the data of Pengra et al., and secondly because it decays via an allowed EC transition that can be calculated comparatively easily.

Metallic magnetic calorimeters (Enss et al., 2000; Fleischmann et al., 2005) are a specific type of cryogenic detector that can be adapted to soft and hard X-ray (Porst et al., 2014; Bates et al., 2016), alpha (Jang et al., 2012), beta (Rotzinger et al., 2008), and optical photon detection. At the Laboratoire National Henri Becquerel (LNE-LNHB), they have been used so far for low energy beta spectrometry (Loidl et al., 2010), as well as for photon spectrometry below 100 keV (Rodrigues and Loidl, 2016). For the measurement of EC probabilities the source is enclosed in the detector absorber. Since all Auger electrons and more than 99.99% of the X-rays emitted by ^{55}Fe are absorbed in the detector, a single line in the energy spectrum is observed for each electron shell on which captures occur. For K captures, the emit-

* Corresponding author.
Email address: martin.loidl@cea.fr (M. Loidl)

https://doi.org/10.1016/j.apradiso.2017.10.042
Received 7 April 2017; Received in revised form 23 October 2017; Accepted 23 October 2017
Available online xxx
0969-8043/

ted radiations (apart from the neutrino) account for 6.539 keV, L captures liberate 769 eV, M captures ~ 84 eV and N captures ~ 8 eV. The energy threshold of MMCs can be as low as a few 10 s of eV, allowing for the detection of K, L and M captures.

2. Metallic magnetic calorimeter setup for the measurement of EC probabilities

Like most cryogenic detectors, metallic magnetic calorimeters (MMCs) are thermal detectors: the energy E of individual particles is measured as a temperature rise $\Delta T = E/C$, where C denotes the total heat capacity of the detector. Since the specific heat of most materials strongly decreases with temperature, the signal ΔT is maximized when operating the detector at very low temperature, in the range 10–30 mK. At the same time, in this temperature range thermodynamic fluctuation noise and other thermal noises are very small. Hence a very high signal-to-noise ratio, and consequently high energy resolution and low energy threshold, are achievable.

For most applications MMCs have a metallic particle absorber, often made of gold. The temperature rise is measured by a metallic paramagnetic thermometer in good thermal contact with the absorber. The name "*metallic* magnetic calorimeters" refers to the metallic nature of the thermometer that is necessary for a fast response. The thermometer is composed of gold or silver and a small concentration of erbium (of the order 0.1%). Its magnetization in the presence of a magnetic field (typically a few mT) strongly varies with temperature. The temperature rise following a particle interaction causes a reduction of the thermometer magnetization. The thermometer is magnetically coupled to a SQUID (Superconducting Quantum Interference Device) magnetometer via a magnetic flux transformer formed by a planar pickup coil and an input coil superimposed to the SQUID sensing loop. SQUIDs operate equally at cryogenic temperatures and are well suited to measure the signal of MMCs with a very low noise level.

In order to restore the initial temperature after each particle interaction, a thermal link connects the detector to a thermal bath maintained at constant temperature. The signal decay time τ_d is determined by the thermal conductance G of the link: $\tau_d = C/G$. Decay times of a few hundred μs to several ms are common, allowing for count rates of the order 10 s^{-1}. The signal rise time τ_r, typically of the order of a few microseconds, depends mainly on the absorber material and dimensions and on the thermal coupling to the thermometer; the intrinsic response time of the thermometer is below a microsecond.

For the measurement of EC probabilities, a low activity ^{55}Fe source was enclosed inside the absorber. The ^{55}Fe was first electroplated on a 3 μm thick gold foil. A 0.44 mm × 0.44 mm square of the source foil, corresponding to ~ 10 Bq, was then sandwiched between the two gold foils (0.48 mm × 0.48 mm × 17 μm each) forming the absorber. In order to tightly enclose the source, the three foils were diffusion welded to each other. Under the influence of the temperature (400 °C) and the mechanical pressure applied for diffusion welding, the gold flowed, and the thickness of the absorber foils diminished to 11 μm on either side of the source foil. This is enough to absorb all Auger electrons, more than 99.997% of the Kα X-rays (5.9 keV) and more than 99.98% of the Kβ X-rays (6.5 keV). These numbers were established via a Monte Carlo simulation using the code PENELOPE (version 2008), probably the most accurate for low energy photon and electron simulation (Salvat et al., 2001). Taking into account the photon emission probabilities, K X-rays escape from the absorber for less than 1×10^{-5} of the K captures.

One advantage of MMCs over other types of cryogenic detectors is that the thermodynamic properties of the paramagnetic temperature sensor are well known and the detector configuration and the operational parameters can be optimized for a given application by calculation. In particular, the geometry of the planar readout coil and the temperature sensor, its erbium concentration and the magnetic field strength can be fixed for a given absorber heat capacity and the temperature that can be reached with a given cryogenic apparatus. The gold-erbium (Au:Er) sensor and the readout coil used in this experiment were conceived for an absorber heat capacity of 4 pJ/K at an operating temperature of 10 mK. The niobium thin film pickup coil forms a meander (see Fleischmann et al. (2005) for an explanation of this coil geometry) covering an octagonal area measuring 237 μm across, with a niobium line width of 2.5 μm and a pitch between neighboring lines of 5 μm. The Au:Er sensor, covering the same area, has a thickness of 1.8 μm and an erbium concentration of 330 ppm.

The absorber described above has a heat capacity of 6 pJ/K at 10 mK. Its initial thickness was chosen larger than assumed when conceiving the sensor since the loss of thickness during diffusion welding had to be taken into account; and the source foil adds an additional heat capacity that was not considered in the sensor design. The corresponding degradation of energy resolution and threshold can be partially compensated by slightly increasing the magnetic field strength.

The absorber was fixed to the thermometer by indium bump bonding: a small piece of indium (~ 40 μm × 40 μm × 20 μm) was placed between the sensor and the absorber, and the absorber was pressed down with a force of ~ 10 N, thus flattening the indium and cold welding it to both the sensor and the absorber. This technique had successfully been used by Croce et al. (2016). Fig. 1b shows the octagonal Au:Er sensor with the small grain of indium on top, in Fig. 1c the absorber is placed on the sensor. The natural radioactivity of indium (beta decay of ^{115}In, $T_{1/2} = 4.4 \times 10^{14}$ y) is not an issue for this measurement: the quantity of indium used (~ 0.1 μg) corresponds to approximately one beta decay per year.

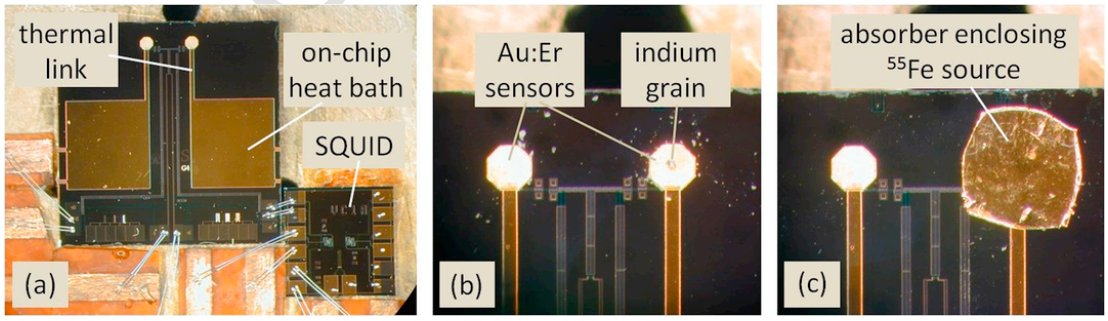

Fig. 1. (a) The MMC chip (5 mm × 5 mm, large square) and the SQUID chip (2.4 mm × 2.4 mm, smaller square). (b) Zoom into the MMC chip with the two octagonal Au:Er sensors, each measuring 237 μm across. On the right hand sensor the indium grain used to bond the absorber to the sensor is visible. (c) The gold absorber enclosing the electroplated ^{55}Fe source has been fixed to the sensor by cold welding with the indium. It is clearly visible that the initially square absorber was deformed during the diffusion welding process.

3. Measurement and results

The output voltage of the SQUID electronics was digitized and recorded continuously during 161 h (~ 7 days). Digital triggering, filtering and pulse height analysis were performed offline. This proved particularly useful in the present experiment since, in addition to a rather large fraction of piled-up pulses, the pulse shapes were not homogeneous and the data analysis had to be adapted.

The pulse rise times were unusually long and varied between ~ 100 μs and 120 μs. This is most likely due to a too large thickness of indium between sensor and absorber. Indium is superconducting at the operating temperature of the MMC and acts as a thermal impedance slowing down the heat transfer from the absorber to the sensor. The variability of the rise times could e. g. arise from a different thermalization speed for athermal phonons entering the indium layer compared to those being thermalized in the gold absorber. The pulse decay time, ~ 4 ms (1/e), was also longer than intended. It was defined by a sputtered gold strip forming the thermal link between the Au:Er sensor and an on-chip heat bath (Fig. 1a) designed for $\tau_d = 1$ ms. However, the decay time depends on the residual resistivity ratio of the gold strip that cannot be predicted precisely and turned out to be lower than expected. The long decay time together with the count rate of 10 s^{-1} lead to a substantial fraction of pulses occurring during the decay of the preceding pulse, and to a non-negligible number of pile-up events. For triggering, a Gaussian filter was used to shorten the pulses. This enables triggering on pulses separated by much less than the pulse decay time. An extendable dead time was then applied.

For the pulse height analysis, a template fit was applied to the triggered pulses, which were for this step filtered by a low-pass instead of the Gaussian filter. A rather short pulse template, 1 ms before and 1 ms after the trigger, was chosen. This proved the best way to determine the pulse heights with high energy resolution in presence of a large fraction of piled-up pulses. Subsequently, a chi square – vs – pulse height plot was used to visualize and reject populations of events affected mainly by the two following phenomena:

(i) To ensure no M capture events were missed, a very low trigger threshold had to be chosen. Therefore, a certain number of events correspond to noise triggers. If a pulse occurs within 1 ms after a noise trigger, it falls into the duration of the template fit and, depending on the delay after the trigger, a pulse height anywhere between the noise level and the true pulse height will be determined. A criterion on the minimum duration of the pulses above the trigger level eliminates most of these events. Only events with the pulse onset very soon after the noise trigger remain. However, in this case the pulse height is only marginally reduced and the pulse will appear in the appropriate peak in the spectrum.

(ii) The second kind of potentially problematic events that can be identified via the chi square – vs – pulse height plot are normally triggered pulses followed by a second pulse within the pulse template window, i. e. separated by less than 1 ms. Most of these events can be removed by a cut on the chi square values. But if the second pulse occurs just after the trigger of the first pulse, or just before the end of the template window, the chi square value is practically normal and these events are not removed. Double-K, L or M pulses that survive the chi square cut are easily identified by their pulse height corresponding to nearly twice the K, L or M energy. But some of the L captures following an M capture may be identified as L captures in terms of pulse height, whereas the trigger event was an M capture. Likewise, K captures following an L or M capture may be identified as K captures, whereas the trigger event was an L or M capture.

The number of these problematic events surviving the chi square cut can in principle be reduced by shortening the pulse template. However, although the pulse rise time (10 – 90%) is about 100 μs, the pulse maximum occurs at around 500 μs and the pulse just begins to decay at 1 ms. Shortening the pulse template will therefore quickly deteriorate the pulse height determination.

Fig. 2 shows the energy spectrum generated from the pulse heights on a logarithmic energy scale. The K, L and M captures are very well separated; also the separation of the M captures from the noise appearing below ~ 40 eV is rather clear. A low energy tail is visible in each of the populations, particularly pronounced in the K capture peak. This is most likely due to the fact that Auger electrons lose part of their energy in the source layer, formed by iron oxide/hydroxide. This energy is not entirely converted to measurable heat (McCammon et al., 1986). Smaller populations of events are observed on the high energy side of each line. Some of these events are unresolved pileup events. The fact that these populations do not extend to higher chi square values in the chi square – vs – pulse height plot indicates that the number of unresolved pileup events is small. Part of the events both on the high and low energy side of the peaks are due to the inhomogeneous time struc-

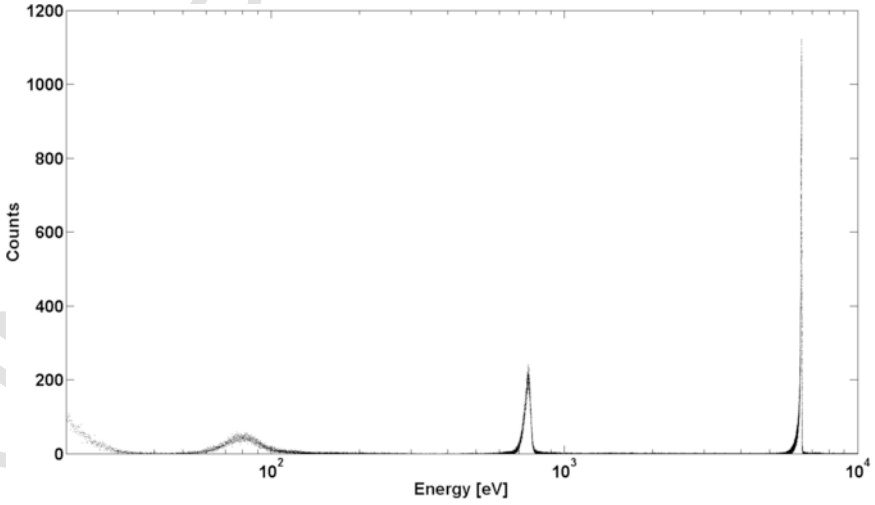

Fig. 2. Total emission spectrum of an electroplated ^{55}Fe source embedded in the absorber of an MMC. The peak at 6.5 keV corresponds to K captures, the peak at 770 eV to L captures and the peak at 80 eV to M captures. The events below ~ 40 eV are noise triggers. The upper limit of this noise event population, i. e. 40 eV, can be considered as the actual energy threshold of this detector. The separation of the M captures from noise is satisfactory.

ture of the pulses interfering with the pulse height analysis. A few of the events on the high energy side of the peaks could also be due to two-hole states in the daughter atom (Robertson, 2015).

To determine the K, L and M peak areas, each population was fitted using the spectrum analysis program Colegram developed at LNHB. Due to the physics involved with the 4π detection in MMCs, the peaks have shapes that cannot be reproduced by any single peak shape available for fitting (different peak shapes with and without tails are available) and several peaks had to be placed arbitrarily within the left and right tails. This made it possible to reproduce very well the peak shapes and to determine the peak areas with small errors.

The peak areas correspond to capture probability ratios P_L/P_K = 0.1134 (25), P_M/P_K = 0.01715 (45) and P_M/P_L = 0.1513 (52). The quoted uncertainties (k = 1) are composed of the statistical uncertainties related to the peak areas and an estimation of the uncertainty due to the data analysis. This was done by varying different parameters: the amount of dead time, more or less severe cuts on chi square, noise trigger suppression on/off, and analysis of subsets of the acquired data. It was verified that the P_K, P_L and P_M values resulting from these analyses are distributed uniformly (rectangular distribution of width w_i) and the corresponding uncertainties were estimated as $w_i/\sqrt{12}$. The values of P_L/P_K and P_M/P_L are in agreement within the uncertainties with the experimental values P_L/P_K = 0.117 (1) and P_M/P_L = 0.157 (3) reported by Pengra et al.

Without the possibility to measure the N captures, whose energy (~ 8 eV) is far below the threshold of the MMC, no absolute capture probabilities can be directly determined. However, given the small N capture probability, using the recommended value for P_N = 0.0006 (2) (Bé et al., 2006) the relative K, L and M capture probabilities can be translated to absolute probabilities whose errors owing to the potential error of P_N should be rather small. The corresponding probabilities from the data of this measurement are then P_K = 0.8840 (26), P_L = 0.1002 (22) and P_M = 0.01516 (38). Here, the quoted uncertainties are composed of the statistical uncertainties related to the peak areas, the uncertainty on P_N, and the estimation of the uncertainty due to the data analysis. The values of P_K, P_L and P_M are in agreement within the uncertainties with the recommended values P_K = 0.8853 (16), P_L = 0.0983 (13) and P_M = 0.0157 (6) from Bé et al. (2006), based on calculation. For comparison, the values of P_L/P_K and P_M/P_L from Pengra *et al.* were translated to absolute probabilities using P_N = 0.0006 (2). The resulting values P_K = 0.881 (4), P_L = 0.103 (4) and P_M = 0.0155 (8) are also in agreement with our new MMC data.

The recent calculations of the ^{55}Fe capture probabilities by Mougeot yield P_K = 0.87717 (35), P_L = 0.10370 (23), P_M = 0.01771 (11) and P_N = 0.001420 (11) (Mougeot, these proceedings). P_N differs substantially from the recommended value in Bé et al. In order to compare our MMC data with Mougeot's results, the MMC values for P_K, P_L and P_M were recalculated using P_N = 0.001420 (11). The resulting values P_K = 0.8833 (26), P_L = 0.1001 (22) and P_M = 0.01515 (38) differ slightly from Mougeot's figures, ~ 2σ for P_K and P_L, and ~ 5σ for P_M. The fact that the recalculated MMC values differ only very slightly from those using P_N = 0.0006 shows that they are rather insensitive to the actual P_N value.

As mentioned above, the energy of the N captures (~ 8 eV) is far below the energy threshold of this MMC. Although MMCs or other cryogenic detectors can be made with a threshold low enough to detect energies as low as 8 eV, there is little hope to be able to detect simultaneously K, L, M and N captures with a reasonably high efficiency. Considering an optimized MMC, the required energy threshold could be achieved only with an absorber heat capacity corresponding to a volume of ~ 2 × 11 μm (the required minimum thickness) × 50 μm × 50 μm. So the source would need to be limited to a diameter of ~ 25 μm, which seems difficult to achieve with available source fabrication techniques.

4. Conclusion

It is the first time that a cryogenic detector has been used for the measurement of the ratios of electron capture probabilities. This new measurement technique has the advantage that it does not rely on i) the knowledge of the fluorescence yields, as is the case for several other measurement techniques, or ii) any other data of questionable reliability. It is furthermore, to our knowledge, the only measurement of P_L/P_K and P_M/P_L of ^{55}Fe since the work of Pengra et al. in 1972. The detector, a metallic magnetic calorimeter with an electroplated ^{55}Fe source embedded inside the absorber, has an energy threshold below 50 eV, low enough to clearly separate the M captures from noise. The measured capture probabilities are in agreement within the uncertainties with the data of Pengra et al. (1972) and with the recommended values in Bé et al. (2006). It has to be stated, though, that a substantial fraction of the events suffer from pile-up. Although a considerable effort was made to eliminate misidentified events, i. e. events whose pulse heights are badly determined and shift the events into one of the other peaks, some of these events have certainly survived the cuts. On the other hand it is possible that a non-negligible number of good events were eliminated by the cuts and thus affect the determined capture probabilities. A new measurement, with a lower source activity and a shorter pulse decay time, thus reducing the difficulties in the data analysis, will shortly be performed.

References

Bates, C., Pies, C., Kempf, S., Hengstler, D., Fleischmann, A., Gastaldo, L., Enss, C., Friedrich, S., 2016. Direct Detection of Pu-242 with a Metallic Magnetic Calorimeter Gamma-Ray Detector. J. Low Temp. Phys. 184, 351–355.

Bé, M.-M., Chisté, V., Dulieu, C., Browne, E., Baglin, C., Chechev, V., Kuzmenko, N., Helmer, R., Kondev, F., MacMahon, D., Lee, K.B., 2006. Table of Radionuclides, Monographie BIPM-5. 3, (ISBN 92-822-2218-7).

Croce, M.P., Hoover, A.S., Rabin, M.W., Bond, E.M., Wolfsberg, L.E., Schmidt, D.R., Ullom, J.N., 2016. Quantitative Analysis of Plutonium Content in Particles Collected from a Certified Reference Material by Total Nuclear Reaction (Q Value) Spectroscopy. J. Low Temp. Phys. 184, 938–943.

Enss, C., Fleischmann, A., Horst, K., Schönefeld, J., Sollner, J., Adams, J.S., Huang, Y.H., Kim, Y.H., Seidel, G., 2000. Metallic Magnetic Calorimeters for Particle Detection. J. Low Temp. Phys. 121 (3–4), 137–176.

Fleischmann, A., Enss, C., Seidel, G., 2005. Metallic Magnetic Calorimeters. In: Enss, C. (Ed.), Cryogenic Particle Detectors. Topics Appl. Phys 99, Springer Berlin, Heidelberg, pp. 151–216.

Jang, Y.S., Kim, G.B., Kim, K.J., Kim, M.S., Lee, H.J., Lee, J.S., Lee, K.B., Lee, M.K., Lee, S.J., Ri, H.C., Yoon, W.S., Yuryev, Y.N., Kim, Y.H., 2012. Development of decay energy spectroscopy using low temperature detectors. Appl. Radiat. Isot. 70, 2255–2259.

Loidl, M., Rodrigues, M., Censier, B., Kowalski, S., Mougeot, X., Cassette, P., Branger, T., Lacour, D., 2010. First measurement of the beta spectrum of ^{241}Pu with a cryogenic detector. Appl. Radiat. Isot. 68, 1454–1458.

McCammon, D., Juda, M., Zhang, J., Kelley, R.L., Moseley, S.H., Szymkowiak, A.E., 1986. Thermal detectors for high resolution spectroscopy. IEEE Trans. Nucl. Sci. 33, 236–239.

Mougeot, X. A New Code for Improved Calculations of Electron Capture Transitions, these proceedings.

Pengra, J.G., Genz, H., Renier, J.P., Fink, R.W., 1972. Orbital-Electron-Capture Ratios in the Decay of ^{55}Fe. Phys. Rev. C 5, 2007.

Porst, J.-P., Bandler, S.R., Adams, J.S., Balvin, M.A., Busch, S.E., Eckart, M.E., Kelley, R.L., Kilbourne, C.A., Lee, S.J., Nagler, P.C., Porter, F.S., Sadleir, J.E., Seidel, G.M., Smith, S.J., Stevenson, T.R., 2014. Characterization and Performance of Magnetic Calorimeters for Applications in X-ray spectroscopy. J. Low Temp. Phys. 176, 617–623.

Robertson, R.G.H., 2015. Examination of the calorimetric spectrum to determine the neutrino mass in low-energy electron capture decay. Phys. Rev. C91, 035504.

Rodrigues, M., Loidl, M., 2016. L X-ray satellite effects on the determination of photon emission intensities of radionuclides. Appl. Radiat. Isot. 109, 570–575.

Rotzinger, H., Linck, M., Burck, A., Rodrigues, M., Loidl, M., Leblanc, E., Gastaldo, L., Fleischmann, A., Enss, C., 2008. Beta spectrometry with magnetic calorimeters. J. Low Temp. Phys. 151, 1087–1093.

Salvat, F., Fernández-Varea, J. M. and Sempau, J., 2001. PENELOPE - A code system for Monte Carlo simulation of Electron and Photon transport. Rapport NEA/NSC/DOC (2001) 19.